

# Simulating soil freeze/thaw dynamics with an improved pan-Arctic water balance model

M. A. Rawlins,<sup>1</sup> D. J. Nicolsky,<sup>2</sup> K. C. McDonald,<sup>3,4</sup> and V. E. Romanovsky<sup>2</sup>

Received 30 October 2012; revised 2 July 2013; accepted 15 July 2013.

[1] The terrestrial Arctic water cycle is strongly influenced by the presence of permafrost, which is at present degrading as a result of warming. In this study, we describe improvements to the representation of processes in the pan-Arctic Water Balance Model (PWBM) and evaluate simulated soil temperature at four sites in Alaska and active-layer thickness (ALT) across the pan-Arctic drainage basin. Model improvements include new parameterizations for thermal and hydraulic properties of organic soils; an updated snow model, which accounts for seasonal changes in density and thermal conductivity; and a new soil freezing and thawing model, which simulates heat conduction with phase change. When compared against observations across Alaska within differing landscape vegetation conditions in close proximity to one another, PWBM simulations show no systematic soil temperature bias. Simulated temperatures agree well with observations in summer. In winter, results are mixed, with both positive and negative biases noted at times. In two pan-Arctic simulations forced with atmospheric reanalysis, the model captures the mean in observed ALT, although predictability as measured by correlation is limited. The geographic pattern in northern hemisphere permafrost area is well estimated. Simulated permafrost area differs from observed extent by 7 and 17% for the two model runs. Results of two simulations for the periods 1996–1999 and 2066–2069 for a single grid cell in central Alaska illustrate the potential for a drying of soils in the presence of increases in ALT, annual total precipitation, and winter snowfall.

**Citation:** Rawlins, M. A., D. J. Nicolsky, K. C. McDonald, and V. E. Romanovsky (2013), Simulating soil freeze/thaw dynamics with an improved pan-Arctic water balance model, *J. Adv. Model. Earth Syst.*, 5, doi:10.1002/jame.20045.

## 1. Introduction

[2] Water is a dynamic element of the climate, biology, and biogeochemistry of the Arctic. Evidence has mounted that the arctic system is now experiencing an unprecedented degree of environmental change due largely to climatic warming [Serreze *et al.*, 2000; Hinzman, 2005; White *et al.*, 2007]. Permafrost temperatures have warmed [Christiansen *et al.*, 2010; Romanovsky *et al.*, 2010a, 2010b; Smith *et al.*, 2010] and active-layer thicknesses have increased in many regions of the Northern Hemisphere [Zhang *et al.*, 2005; Wu and

Zhang, 2010]. There is evidence that the arctic freshwater cycle is intensifying [Peterson *et al.*, 2002, 2006; Rawlins *et al.*, 2010]. Smith *et al.* [2007] documented an increase in minimum daily flows across northern Russia and speculated a connection to reduced soil freezing together with an increase in precipitation. Permafrost is the major control on hydrological dynamics at the local scale [Yoshikawa and Hinzman, 2003]. It is expected that as permafrost continues to degrade the arctic terrestrial freshwater system will transition from a surface water-dominated system to a groundwater-dominated system [Frey and McClelland, 2009]. Advances in understanding of these changes require the continued development of process-based models which accurately capture spatial and temporal dynamics and linkages between key elements of the arctic freshwater system.

[3] The Pan-Arctic Water Balance Model (PWBM), advanced from a more generic Water Balance Model first described by Vörösmarty *et al.* [1989], simulates all major elements of the terrestrial arctic water cycle. It is an implicit daily time step model and is forced at the atmosphere-land surface boundary with meteorological data. In other words, the simulations are analogous to

<sup>1</sup>Department of Geosciences, University of Massachusetts, Amherst, Massachusetts, USA.

<sup>2</sup>Geophysical Institute, University of Alaska Fairbanks, Fairbanks, Alaska, USA.

<sup>3</sup>Department of Earth and Atmospheric Sciences, City College of New York, City University of New York, New York, USA.

<sup>4</sup>Jet Propulsion Laboratory, California Institute of Technology, Pasadena, California, USA.

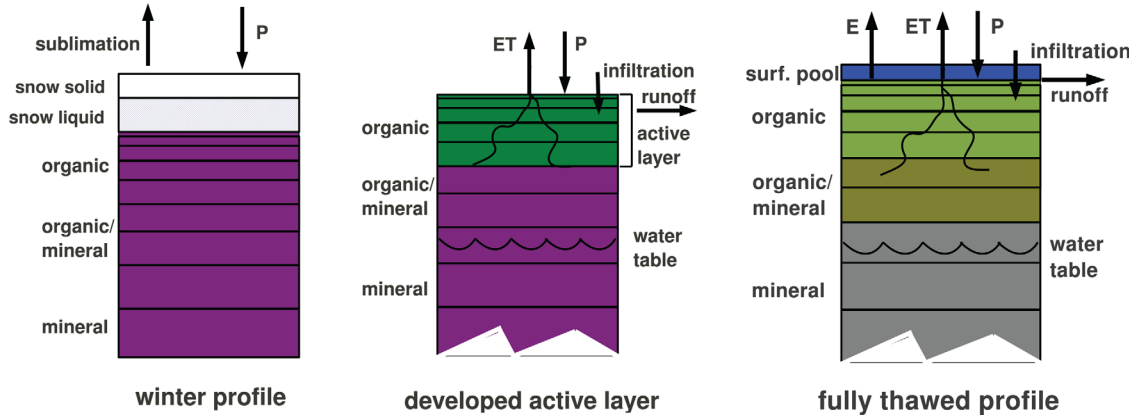


**Figure 1.** Schematic of PWBM soil profiles for winter (left), spring (center), and summer (right). Transitions back to frozen condition during autumn not shown. The model develops an active layer in spring which allows for water gains through infiltration and losses from runoff and evapotranspiration (ET). Water pools on the surface if infiltration capacity is exceeded. Drainage between layers follows Darcy’s Law as solved through the Richard’s equation. The model incorporates subgrid scale open water extents. Temporally varying change in water table height is also simulated.

an offline simulation by an uncoupled LSM. It has been used to investigate causes behind the record Eurasian discharge in 2007 [Rawlins *et al.*, 2009], to corroborate remote sensing estimates of surface water dynamics [Schroeder *et al.*, 2010], and to quantify present and future water cycle changes in the area of Nome, Alaska [Clilverd *et al.*, 2011]. In a comparison against observed river discharge, PWBM-simulated SWE fields compared favorably [Rawlins *et al.*, 2007]. The updated version of PWBM described here follows on improvements to the Community Land Model (CLM) as outlined in Nicolsky *et al.* [2007]. Structurally, the prior version of PWBM differed from this new updated version in two key ways: (i) it contained only two soil layers (rooting zone, deep soil zone) and (ii) active-layer evolution was estimated using the Stefan solution of the heat-transfer problem. The Stefan solution requires estimation of empirically derived landcover-specific parameters known as “edaphic factors” to convert accumulated energy (e.g., thawing degree days) into a depth of thaw given the specific thermal properties of local vegetation and soils.

[4] It has been demonstrated that numerical model simulations of soil freezing and thawing require attention to several key processes operating across the landscape [Nicolsky *et al.*, 2007; Lawrence and Slater, 2008; Rinke *et al.*, 2008; Schaefer *et al.*, 2011]. For example, thermal and hydrological properties of organic and mineral soils differ considerably. Improvements in permafrost distribution, active-layer thickness, and deep ground temperatures have been documented in the CLM4 [Lawrence *et al.*, 2012]. Swenson *et al.* [2012] described modifications to CLM4 hydraulic permeability when soils are frozen which corrected a dry bias. Upgrades as well have been made to the SiBCASA model, including the addition of parameterizations which account for the effect of depth hoar and wind compaction on simulated snow density [Schaefer *et al.*,

2009]. Wisser *et al.* [2011] described model improvements which centered on the explicit representation of peatlands and their associated properties. Jiang *et al.* [2012] explored the effects of climate change and fire on soil temperatures using a soil thermal model that couples heat and water transport.

[5] The present paper centers on descriptions of new components and analysis of results from an improved version of Pan-Arctic Water Balance Model (PWBM). Upgrades to the model enable more physically based simulations of snow and soil dynamics. Our primary domain is the pan-Arctic drainage basin. Grid resolution is the  $25 \times 25 \text{ km}^2$  version of the northern hemisphere Equal Area Scalable Grid (EASE-Grid). Following a description of the model and data sources, our analysis begins with comparisons between simulated and observed soil temperatures for four sites in Alaska. We then evaluate results and explore model performance at the pan-Arctic scale. Lastly, we use projections for future precipitation and air temperature for a representative location in central Alaska to investigate potential changes in the soil regime and connections with expected climatic changes.

## 2. Modification to the PWBM

### 2.1. Soil Model

[6] Figure 1 depicts a schematic representation of the updated PWBM described in this paper. The updated PWBM soil model discretizes a 60 meter soil column which contains 23 layers, with layer thickness increasing with depth. The model simulates snow/ground temperature dynamics in a more physically based manner, using the 1-D heat equation with phase change

**Table 1.** Soil Parameters Used in the PWBM Simulations<sup>a</sup>

Soil Type	$\lambda$ (W m <sup>-1</sup> K <sup>-1</sup> )	$C$ (J m <sup>-3</sup> K <sup>-1</sup> × 10 <sup>6</sup> )	$\Theta_{sat}$	$k_{sat}$ (m s <sup>-1</sup> × 10 <sup>-3</sup> )	$\Psi_{sat}$ (mm)	$\beta$
Sand	$\lambda_m = 3.6$	$C_m = 3.0$	0.25	0.023	-47	3.4
Loam	$\lambda_m = 3.0$	$C_m = 3.0$	0.35	0.042	-207	6.1
Clay	$\lambda_m = 2.3$	$C_m = 3.0$	0.45	0.020	-390	12.1
Sandy loam	$\lambda_m = 3.3$	$C_m = 3.0$	0.40	0.071	-132	4.5
Clay loam	$\lambda_m = 2.6$	$C_m = 3.0$	0.39	0.028	-289	8.2
Organic soil	$\lambda_o = 1.5$	$C_o = 1.9$	0.9	0.02	-120	2.7

<sup>a</sup>Each grid cell in the model is characterized by one of the five mineral soil types. Model parameters are defined through a weighted combination of organic and mineral soil properties. See *Rawlins et al.* [2003] for more detail on the PWBM soil routine.

$$C \frac{\partial T}{\partial t} + L \zeta \frac{\partial \theta}{\partial t} = \frac{\partial}{\partial z} \left( \lambda \frac{\partial T}{\partial z} \right), \quad z \in [z_s, z_b] \quad (1)$$

and diffusive and gravitational movement of water in thawed ground by solving Richard’s equation

$$\frac{\partial \zeta}{\partial t} = \frac{\partial}{\partial z} \left( k \left[ \frac{\partial \psi}{\partial z} + 1 \right] \right), \quad z \in [0, z_b]. \quad (2)$$

[7] Here  $T = T(z, t)$  is the temperature,  $\zeta = \zeta(z, t)$  is the volumetric water content,  $\psi = \psi(z, t)$  is the soil matrix potential. The quantities  $C = C(T, z)$  [Jm<sup>-3</sup>K<sup>-1</sup>] and  $\lambda = \lambda(T, z)$  [Wm<sup>-1</sup>K<sup>-1</sup>] represents the volumetric heat capacity and thermal conductivity of soil, respectively;  $L$  [Jm<sup>-3</sup>] is the volumetric latent heat of fusion of water, and  $\theta = \theta(T, z)$  is the so-called “unfrozen liquid pore water” fraction, and  $k = k(T, z)$  is the hydraulic conductivity. Details of the numerical solution of the heat equation can be found in Appendix A. The interested reader may consult the CLM 4.0 technical description for details of the numerical solution of the Richard’s equation. The equations are solved implicitly with a daily time step. At the upper boundary condition air temperature and precipitation are prescribed as described below. We emphasize that equation (2) is applicable only for the thawed ground material. In order to extend to simulations of water motion in frozen ground, some models (e.g., CLM 4.0 [Oleson et al., 2010]) propose that  $\psi = \psi(T, \theta, x)$  if  $T < T_p$ , where  $T_p$  is the so-called freezing-point temperature depression. In this work, we assume that the water migration in the frozen ground is negligibly small. The latter can be modeled by assuming that the coefficient of hydraulic conductivity  $k(T, z) = 0$ , if  $T < T_p$ . Thus, when a layer of the ground material becomes frozen the total water content  $\zeta$  in it stays constant until the moment when the layer becomes thawed again. Note that for frozen soil layers the matric potential can be arbitrarily defined, since it does not enter into calculations, and the water flux boundary condition is imposed at the bottom of the thawed region. Another distinction of the proposed model from the CLM is the way soil thermal properties are parameterized. Additional information is provided in Appendix A.

## 2.2. Snow Model

[8] Seasonal snow cover has a significant influence on the ground thermal regime [Zhang, 2005]. For example,

snowcover provides an insulating layer and limits the degree of soil cooling during cold winter months. Classification maps derived from wind, precipitation, and air temperature data [Sturm et al., 1995] can be used to infer snow thermal and physical properties for simulations with numerical models. Land surface models (LSMs) capable of simulating soil freeze/thaw dynamics have recently begun to focus on the effects of snow on underlying soil temperatures.

[9] Formulations in the PWBM for snow accumulation, sublimation, melt, and associated processes are described in *Rawlins et al.* [2003]. The simulated snowpack contains both a solid and a liquid portion, providing a total model estimate for snow water equivalent (SWE). New routines to account for seasonal changes in snow density follow on recent improvements to the CLM and to the Simple Biosphere/Carnegie-Ames-Stanford Approach (SiBCASA). The CLM version 4 includes a snow model which simulates processes such as accumulation, melt, compaction, snow aging [Lawrence et al., 2012]. The Simple Biosphere/Carnegie-Ames-Stanford Approach (SiBCASA) uses the snow classification system of Sturm et al. [1995], and a snow model derived from the CLM. We take here a similar approach in modeling the temporal evolution in snowpack density. Details of our new snow density model are described in Appendix A.

## 2.3. Organic Content and Parameterizations

[10] In many parts of the Arctic where soil carbon is high, the first 40–50 cm of soil is nearly 100% organic, with a transition from organic to mineral soil and 100% mineral soil below. In the middle transition zone, thermal and hydraulic properties of mixed mineral and organic soil material can be approximated as a weighted combination of the mineral soil and organic soil properties. As described in *Rawlins et al.* [2003], the previous version of PWBM contained an upper organic layer and a lower mineral layer imposed in the two layer profile.

[11] In order to better account for the thermal and hydrologic properties of soils, we parameterized carbon density in each soil layer. We take a similar but not identical approach to the one described in *Lawrence and Slater* [2008]. The Global Soil Data Task (GSDT, 2000) data set contains soil-carbon density ( $C$ , kg m<sup>-3</sup>) across the depth interval of 0–1 m. To obtain  $C$  across the pan-Arctic basin, we averaged the five arc-second GSDT data for each EASE-Grid cell. We applied the soil profile for polar and boreal soils from *Zinke et al.*

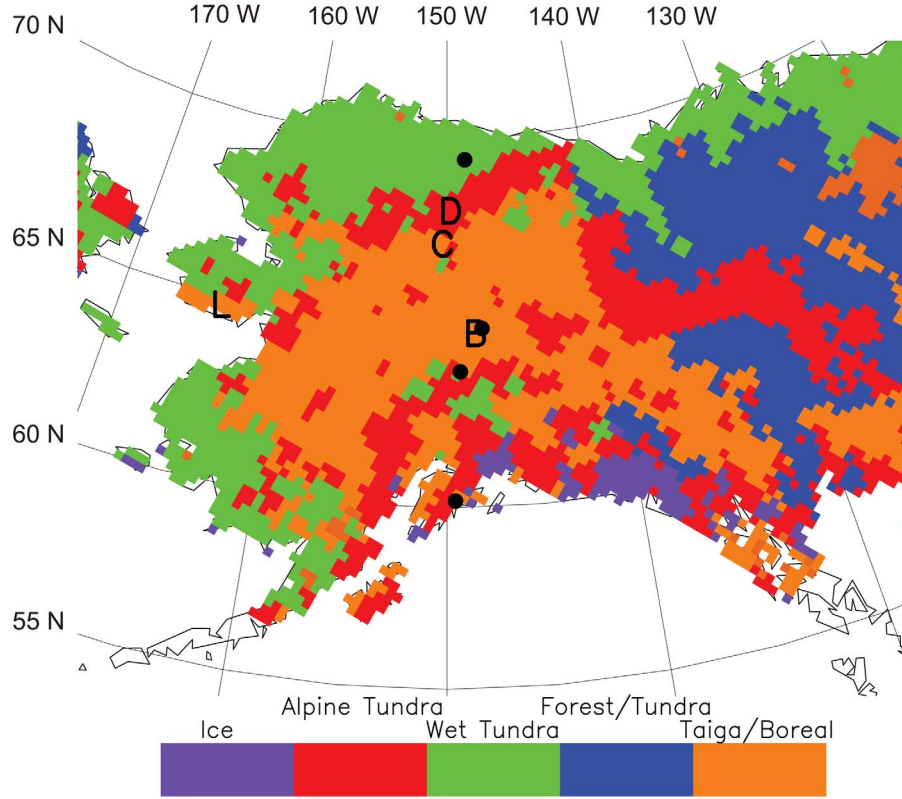


**Figure 2.** Research sites used for model evaluations: Bonanza Creek (B); Coldfoot (C); Council (L); Dietrich (D). Bonanza Creek, Coldfoot, and Dietrich are in the Alaska Ecological Transect (ALECTRA) network. Filled circles mark other ALECTRA sites. Landcover units within each respective site are listed in Table 2. Colors denote landcover class <http://ecosystems.mbl.edu/tem/GIS/Veg/temveg.htm> on the  $25 \times 25 \text{ km}^2$  EASE-Grid used in the simulations.

[1986] to obtain carbon storage over the top 11 model soil layers (1.4 m depth). Soil carbon or organic fraction for each layer was then determined as

$$f_{sc,i} = \rho_{sc,i} / \rho_{sc,max} \quad (3)$$

where  $f_{sc,i}$  is the carbon fraction of each layer  $i$ ,  $\rho_{sc,i}$  is the soil carbon density, and  $\rho_{sc,max}$  is the maximum possible value (peat density of  $130 \text{ kg m}^{-3}$ , Farouki [1981]). Soil properties for each layer are specified as a weighted combination of organic and mineral soil properties

$$\mathcal{P} = (1-f)\mathcal{P}_m + f\mathcal{P}_o \quad (4)$$

where  $f$  is the fraction of organic material in the soil layer,  $\mathcal{P}_m$  is the value for mineral soil,  $\mathcal{P}_o$  is the value for organic soil, and  $\mathcal{P}$  is the weighted average quantity. Thermal and hydrologic parameters as a function of soil class are listed in Table 1.

### 3. Data Sets

#### 3.1. Forcing Data

[12] Many of the static input data fields (e.g., soil properties, landcover type, and snow class) and meteor-

ological forcings used in the prior and present version of the PWBM are available within the ArcticRIMS project archive (<http://rims.unh.edu/>). For the two pan-Arctic simulations, we draw daily 2 m air temperature, precipitation, and wind speed from two atmospheric reanalyses data sets. Atmospheric reanalyses are retrospective forms of numerical weather prediction using a fixed model and data assimilation system. The first (hereafter referred to as NNR) was derived from the NCEP/NCAR (National Centers for Environmental Prediction/National Center for Atmospheric Research) effort [Kalnay *et al.*, 1996] (in ArcticRIMS see: [http://rims.unh.edu/data/read\\_me.cgi?category=7&subject=0](http://rims.unh.edu/data/read_me.cgi?category=7&subject=0) and [http://rims.unh.edu/data/read\\_me.cgi?category=2&subject=0](http://rims.unh.edu/data/read_me.cgi?category=2&subject=0)). The second set of reanalysis data (hereafter ERA-40) was drawn from the European Center for Medium Range Weather Forecasts (ECMWF) ERA-40 reanalysis [Uppala *et al.*, 2005] (in ArcticRIMS see: [http://rims.unh.edu/data/read\\_me.cgi?category=7&subject=8](http://rims.unh.edu/data/read_me.cgi?category=7&subject=8) and [http://rims.unh.edu/data/read\\_me.cgi?category=2&subject=5](http://rims.unh.edu/data/read_me.cgi?category=2&subject=5)). No ERA-40 wind speed data is available in Arctic-RIMS and so NNR wind speed are used in their place for the simulations described below.

[13] Across the terrestrial Arctic, total precipitation over cold season months can be used as a proxy for

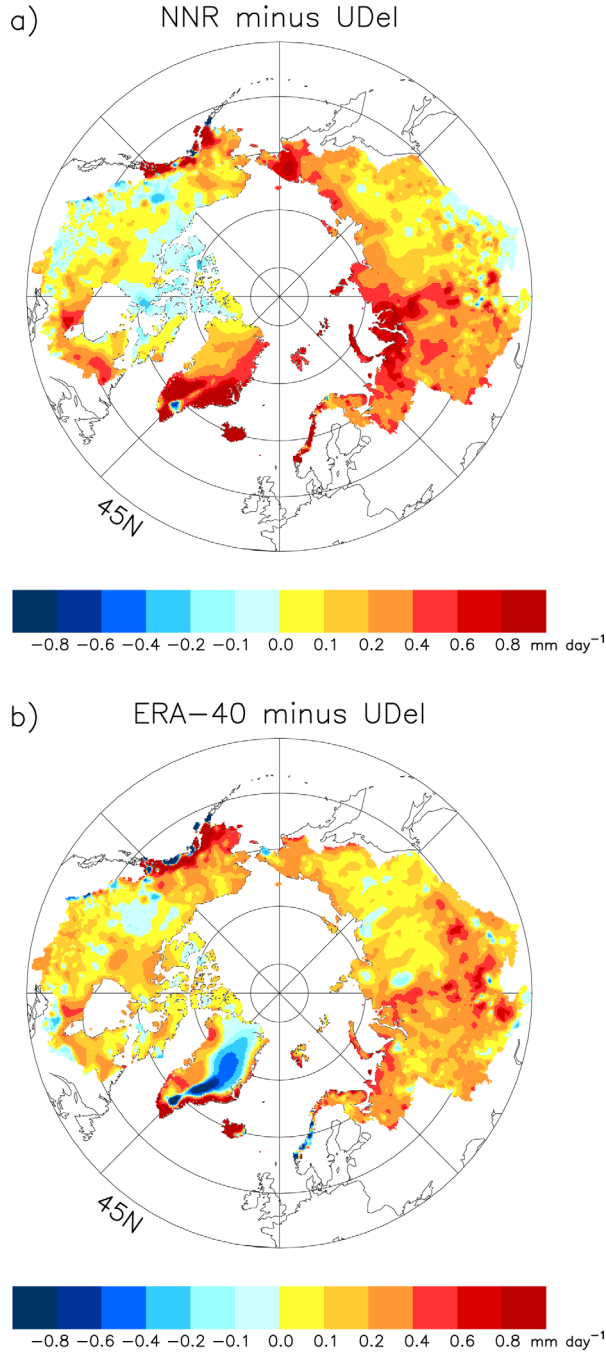


**Figure 3.** Bias in cold season (Nov–Apr) precipitation at each  $25 \times 25$  km<sup>2</sup> EASE-Grid across the pan-Arctic drainage basin. Bias is defined as the difference between the reanalysis and observed (UDeI) precipitation totals.

snowfall. As a first step, we assessed biases in NNR and ERA-40 total precipitation for November–March using precipitation data available from the University of Delaware (UDeI) [Matsuura and Willmott, 2009; Willmott and Matsuura, 2000]. The UDeI data sets were developed through interpolations of meteorological station data records. For this assessment, average November–March precipitation was taken over the period 1980–1999. Bias maps are shown in Figures 2a and 2b. The distribution of biases is largely positive across the pan-Arctic. Integrated area average biases (excluding Greenland) are 0.17 and 0.24 mm day<sup>-1</sup> for NNR and ERA-40, respectively. Across Alaska, biases are also mostly positive. For the region west of 135°W, averages are 0.21 mm day<sup>-1</sup> for NNR and 0.31 mm day<sup>-1</sup> for ERA-40.

### 3.2. Ground-Based Validation Data

[14] Evaluations of model simulated soil temperatures are made using multiple within-site observations from a subset of the Alaska Ecological Transect (ALECTRA) sites (Figure 3). We chose ALECTRA sites that have sufficient multiyear data over the period 2000–2005. The evaluation sites are Bonanza Creek, Coldfoot, and Dietrich (Table 2). Missing data due to logger or sensor issues limit the number of sites available for examination. The ALECTRA sites were conceived and implemented to capture spatial heterogeneity in soil and vegetation stem/branch temperature conditions across the landscape that largely reflect microclimatic variability. Many of the ALECTRA sites are situated near research stations where meteorological observations are available. The sites are distributed along a north-south latitudinal transect extending from Arctic coastal tundra through the boreal and into maritime forest. Soil temperature and snow data for Council were drawn from records archived at the University of Alaska Water and Environment Research Center (<http://ine.uaf.edu/werc/>). For the simulations at each of the four research sites (Table 2), we used the average 2 m air temperatures across available sites. Precipitation and wind speed were drawn from the NNR.

[15] Observations of ALT from the Circumpolar Active Layer Monitoring (CALM) data set [Brown *et al.*, 2000] are used to evaluate PWBM simulated estimates. Field sampling in the CALM program typically involves measurements across a grid spanning 0.1 km<sup>2</sup> or in some locations 1 km<sup>2</sup> area. Each recorded ALT value represents maximum seasonal depth of thaw of

**Table 2.** Landscape Units Within the Respective Research Sites<sup>a</sup>

Site	Bonanza Creek	Coldfoot	Council	Dietrich
Landscape unit	South slope	South slope	Tundra	South slope
Landscape unit	Black spruce	Black spruce	Spruce	White spruce
Landscape unit	White spruce	Bog	Shrub	Bog
Landscape unit		Willow swamp	Woodland	Creek

<sup>a</sup>Data for Bonanza Creek, Coldfoot, and Dietrich are part of the Alaskan Ecological Transect (ALECTRA).



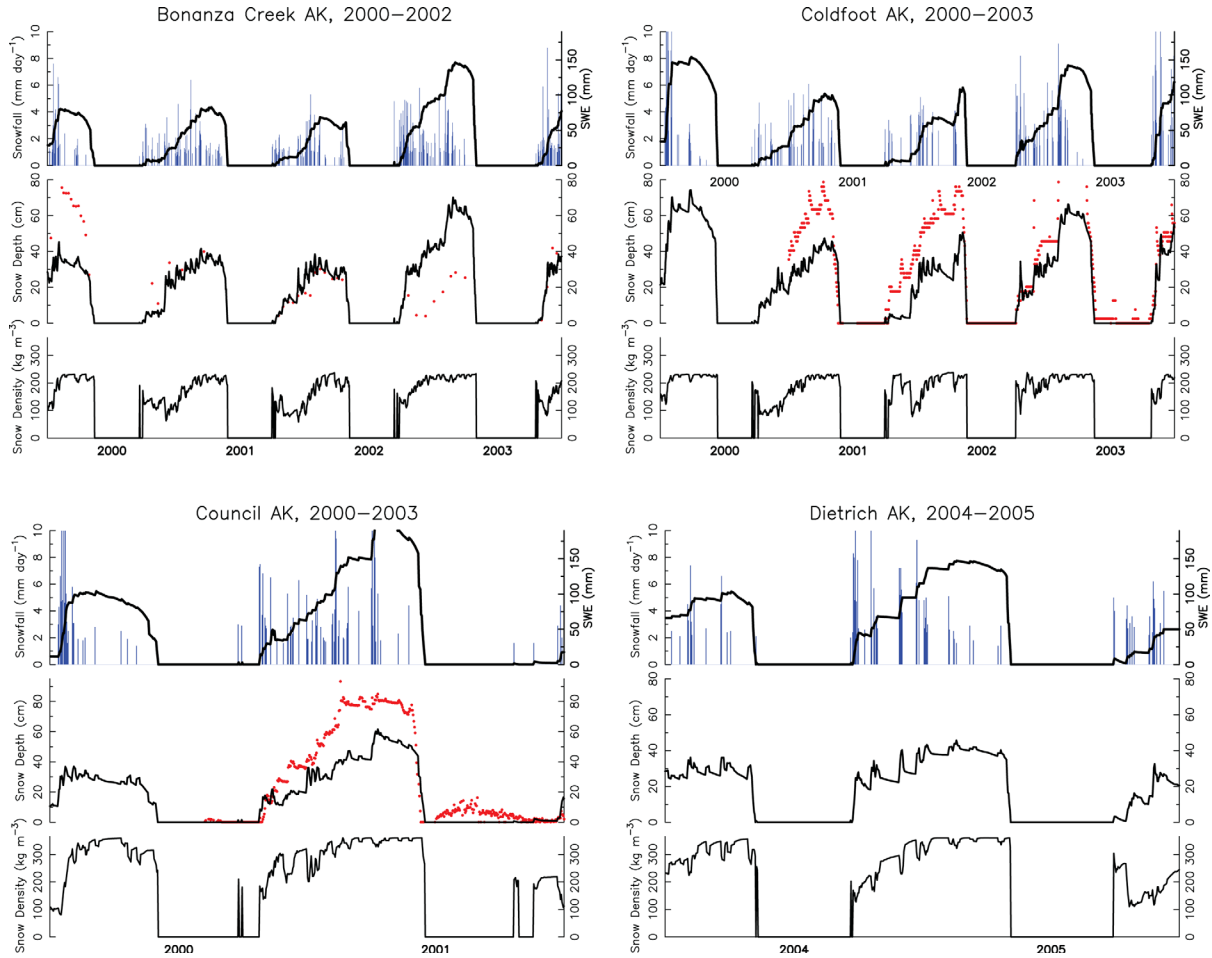


**Figure 4.** Simulated snowfall (vertical bars,  $\text{mm day}^{-1}$ ), snow water equivalent (mm), snow depth (cm), and snow density ( $\text{kg m}^{-3}$ ) for the grid cells encompassing Bonanza Creek, Coldfoot, Council, and Dietrich sites. Available observed snow depths (red dots) shown for the first three sites.

the 121 samples. For our comparisons with PWBM-simulated values, we take the average of all nonmissing CALM ALTs over the period 1980–2011.

## 4. Results

### 4.1. Site Comparisons

[16] Figure 4 shows the simulated snowpack behavior over several years for each of the four study sites. At each site, snow density increases through the cold season, starting at around  $100 \text{ kg m}^{-3}$ . The profiles for Bonanza Creek and Coldfoot are similar, with snow densities spanning a range between 100 and  $250 \text{ kg m}^{-3}$ . A larger range is evident for Dietrich and Council, where end-of-season snow density is over  $300 \text{ kg m}^{-3}$ . Comparing simulated snow depth with observations reveals no consistent biases. In some years, there is good agreement, in some years the model overestimates snow depth, in other years it underestimates. This is worth noting given the positive bias (overestimate) in cold season precipitation (Figure 3).

[17] The thermal conductivity of organic soils is low, ranging from  $0.50 \text{ W m}^{-1} \text{ K}^{-1}$  at saturation to  $0.06 \text{ W}$

$\text{m}^{-1} \text{ K}^{-1}$  under dry conditions [Farouki, 1981]. Figure 5 shows model simulated thermal conductivity profiles for May, June, September, and October at the four sites. For Bonanza Creek, Coldfoot, and Council the simulated organic density as parameterized is nearly 100% in upper 20 cm and transition to fully mineral soil at around 40 cm. Note the much thinner modeled organic horizon for the Dietrich site. Simulated thermal conductivity there increases sharply down to around 30 cm depth where it approaches  $2.4 \text{ W m}^{-1} \text{ K}^{-1}$ . For Dietrich, the reduced thermal conductivity in the soil layer centered at 0.55 m is largely attributable to lesser water content. This soil layer is the lowest that thaws over the spin-up period during which time it loses some water. During the simulation period, permafrost again develops at this layer, however, the water content and thermal conductivity then is lower. At each site, conductivities tend to be higher in spring versus autumn. This result reflects higher soil moisture amounts, and thus thermal conductivity, following spring snowmelt.

[18] Soil temperatures are influenced by a number of climate and landscape factors [Callaghan *et al.*, 2011].

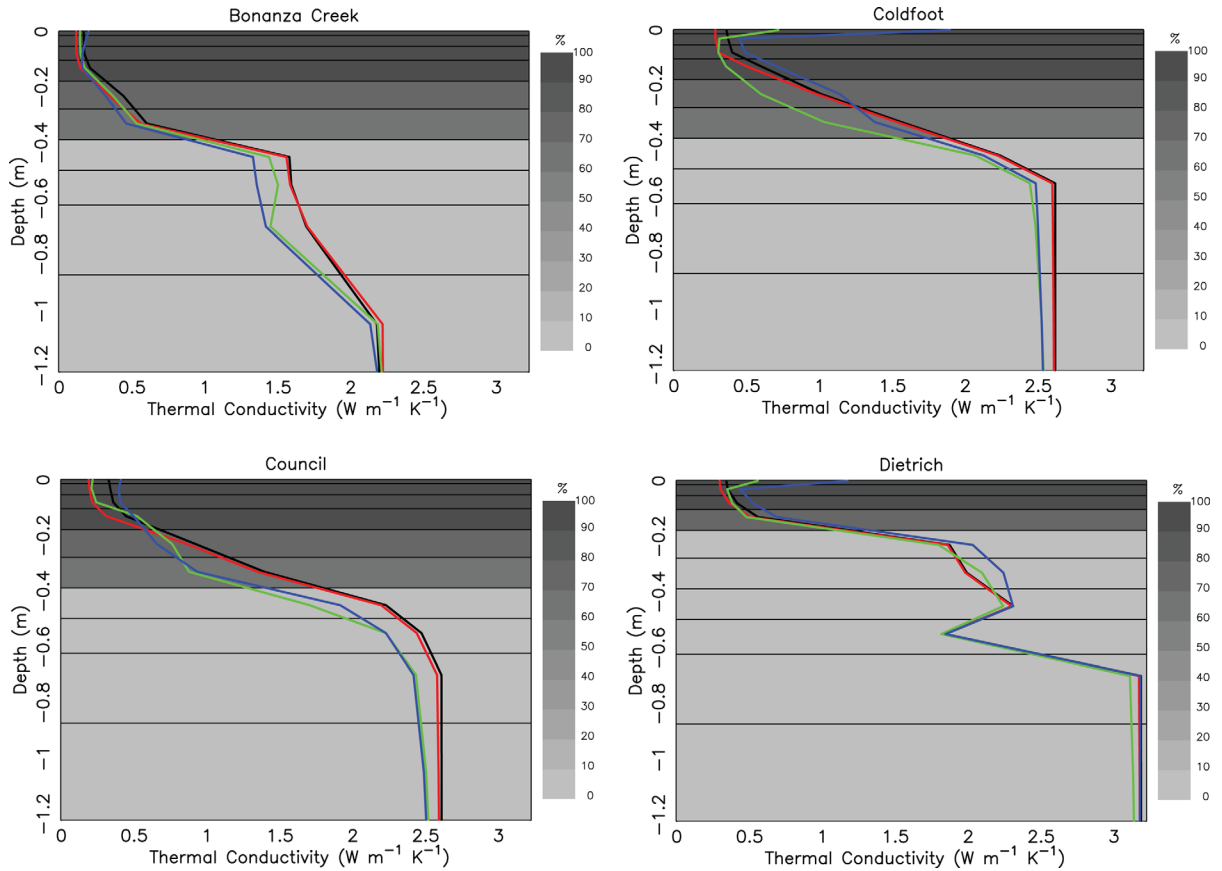


**Figure 5.** Simulated soil thermal conductivity ( $\text{W m}^{-1} \text{K}^{-1}$ ) with depth for the grid cell encompassing Bonanza Creek, Coldfoot, Council, and Dietrich sites for months May (black), June (red), September (green), and October (blue) in 2000 (2001 for Bonanza Creek). Gray shading indicates percent of organic carbon density in each soil layer.

The seasonal cycle in air temperature and seasonal accumulation and melt of snowpack are perhaps the two most important processes that influence annual variations in soil temperatures. Examining simulated soil temperatures against observed data provides insights into model efficacy. Figures 6a and 6b show simulated and observed daily soil temperatures at 25 cm depth for Bonanza Creek and Coldfoot. Colored traces represent temperatures from measurements in each landscape units within the research sites. For Bonanza Creek, model simulated summer temperatures are well captured, falling between the warm south facing slope and the cooler spruce sites. Model temperatures during winter are clearly too warm. At Coldfoot, summer temperatures again are well simulated. In contrast with Bonanza Creek, 25 cm temperatures during the first 5 months of the year fall in the middle of the range of observations.

[19] Figure 7 depicts monthly average soil temperature at both 25 and 50 cm depth for Bonanza Creek, Coldfoot, Council, and Dietrich. For Bonanza Creek, simulated temperatures in summer fall well within the range of the measured data from the three landscape units (Table 2). In winter, the model is warmer than observations, with simulated temperatures at 25 and 50

cm remaining near freezing through the winter. Model simulated snow depth compares well with observations over the winters of 2000–2001 and 2001–2002 (Figure 4). The warm soil temperature bias in winter 2002–2003 is consistent with an overestimation in simulated snow depths. Over the period 1980–2008, precipitation averages  $374 \text{ mm yr}^{-1}$  in the daily NNR data versus  $286 \text{ mm yr}^{-1}$  for National Weather Service observations from Fairbanks International airport over the climate normal period 1971–2000.

[20] For Coldfoot, model simulated soil temperatures at 25 cm depth fall well within the measured range across the landscape units during most months (Figure 7). Simulated snow depths are lower than the observed values in two of the three years shown. The exception is winter 2002–2003 when the model overestimates temperatures. Simulated temperatures at 50 cm depth remain near  $0^\circ\text{C}$  through summer, whereas the observations are  $1\text{--}4^\circ\text{C}$  warmer.

[21] At Council, simulated temperatures are colder than the observations by some  $5^\circ\text{C}$  during the coldest months (Figure 7). Simulated midwinter snow depths in 2000–2001 were approximately half (40 versus 80 cm) of the observed values. This bias could explain some of the discrepancy in simulated soil temperatures. With no

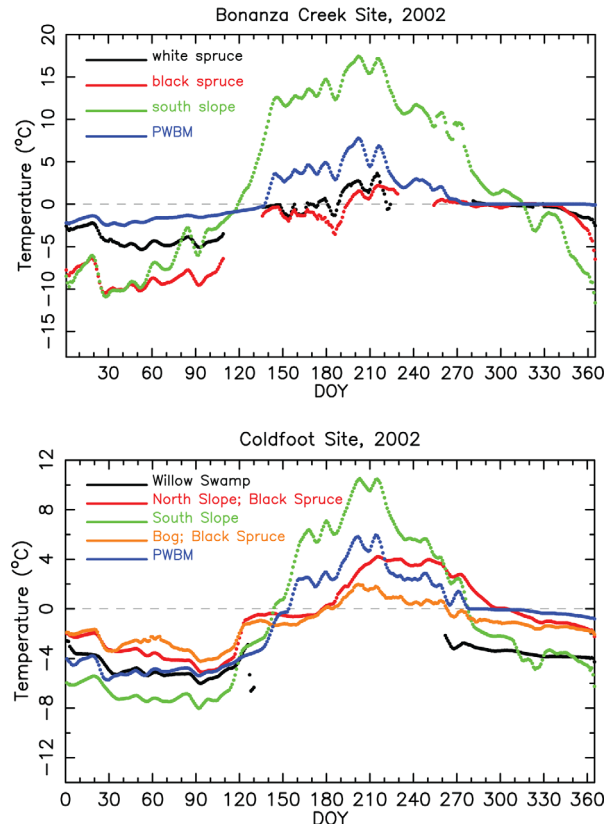


**Figure 6.** Daily soil temperatures at 25 cm depth simulated by the PWBM and from observations at (a) Bonanza Creek and (b) Coldfoot. A 7 day running mean is applied to each time series. Available landscape sites for each location are listed in Table 2.

south facing slope (Table 2), observed temperatures at Council are notably cooler than those at Bonanza Creek and Coldfoot sites. Both the annual temperature cycle and the range in temperatures across the four landscape units at Council are small. Good agreement with the observations occurs in summer each year, where the model and observations at 25 and 50 cm are in the range 0–5°C. The small variations around 0°C in the winter 2000–2001 observations at Council may be a result of a deep snowpack and/or a reflection of a thick organic layer, both of which would tend to limit the influence of the overlying cold winter air.

[22] For Dietrich, simulated temperatures fall within the observed range during most months, excluding spring of 2004 and 2005 when simulated temperatures are approximately 1–2°C colder than the observations (Figure 7). No observed snow depth data are available for Dietrich. Like with Bonanza Creek, Coldfoot, and Council sites, simulated temperatures in summer agree well with observations. When compared with Bonanza Creek, the larger degree of cooling in the Dietrich simulation is largely a reflection of the thinner organic layer and, in turn, higher thermal conductivities (Figure 5).

[23] We performed a series of sensitivity experiments to help elucidate potential sources of bias in simulated soil temperatures at depth during both the cold and

warm season. In particular, we examined the simulated soil temperatures at 25 cm at Bonanza Creek and Council sites. For Bonanza Creek, reducing snowfall over the cold season by 50% cools temperatures at the 25 cm depth over the cold season (November–March, 2001–2000) by 2.3°C. These results suggest that any errors in snow depth can explain some but not all of the bias in simulated winter temperatures at depth. We then analyzed the effect of errors in organic content (by carbon density in the model) of soil layers by decreasing the organic content by 50%. This change resulted in a cooling of temperatures by approximately 1°C. In view of these results, we speculate that a combination of errors in snow depth and organic layer thickness (carbon density) could well explain most of the bias in simulated soil temperatures at depth. For Council, doubling of cold season snowfall warms soil temperatures at 25 cm (1999–2000) by 3.6°C. This result suggests that errors in the approximation of snow depth can explain most but not all of the bias in the simulation results shown in Figure 7.

[24] We also performed a pair of experiments to better understand model sensitivity during the warm season. For these simulations we simultaneously perturbed soil layer carbon density and air temperature and focused on Bonanza Creek sites. First, in order to mimic typical conditions across the south-facing slope, we approximated an organic layer thickness of 20 cm and as described above reparameterized the resultant carbon density of each layer. At the same time, we scaled the input 2 m air temperatures upward by 2°C. In the second sensitivity experiment, we approximate condition in either the white spruce or black spruce stand by parameterizing a 60 cm organic layer and resultant carbon densities at depth, along with 2°C cooler temperatures. A difference of 4.2°C was found between the two simulations. Our results here demonstrate that the numerical soil freezing and thawing scheme, parameterizations and input data for organic content, and input air temperature forcings are able to capture much of the variations in observed summer soil temperatures across the Bonanza Creek sites.

#### 4.2. Simulated Active Layer Thickness and Permafrost Extent Across the Pan-Arctic

[25] To further evaluate model performance, we ran additional simulations across the entire pan-Arctic drainage basin. Model spin-up was performed through 50 iterations over the year 1980, the first year of the transient simulation. We use the daily precipitation, air temperature, and wind data derived from the reanalysis products as described in section 3.1. A grid cell is labeled as containing permafrost if at least one layer within the upper 15 soil layers (3.25 m depth) remains frozen throughout the year. Simulated ALT is estimated as the depth where soil temperature crosses the 0°C threshold. In these evaluations, observed CALM ALT represents all available nonmissing values for a given site over the period 1980–2011.

[26] Figure 8 shows comparisons between simulated and observed ALT over the period 1980–1999 from the



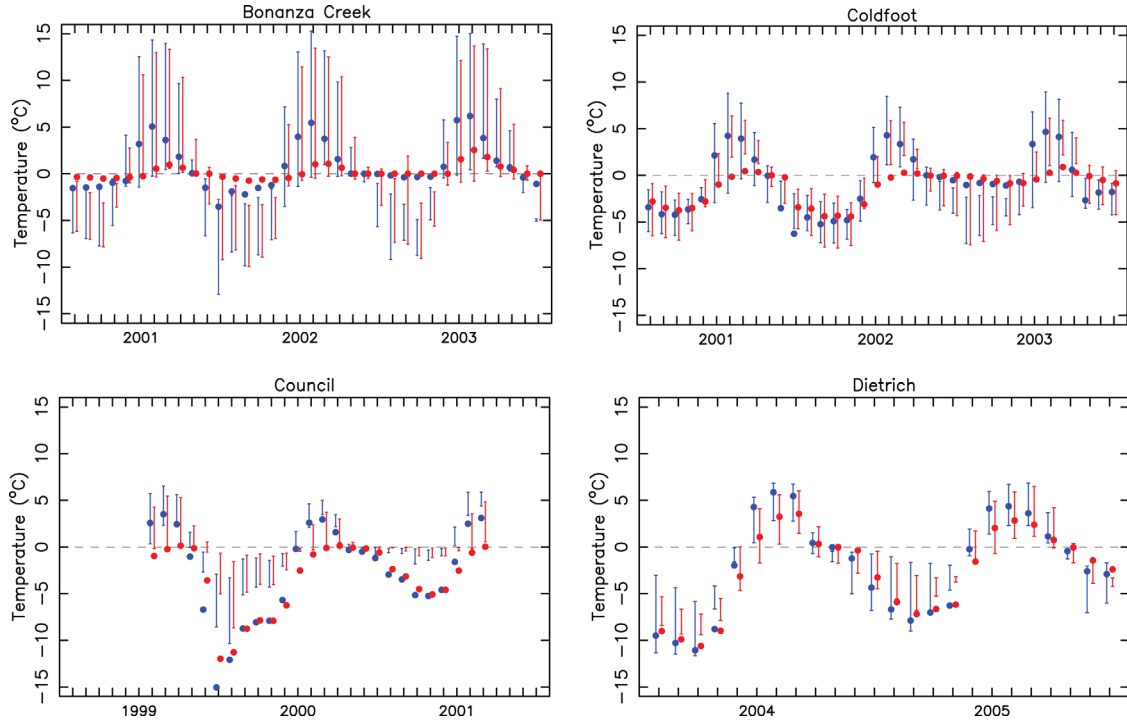


**Figure 7.** Range in monthly soil temperatures at 25 (blue) and 50 cm (red) depth from observations (vertical lines) and model value at each of those depths (circles) across the available landscape units at Bonanza Creek, Coldfoot, Council, and Dietrich. For each month, the first bar/circle represents values for 25 cm and second for 50 cm. Available landscape sites for each location are listed in Table 2.

prior (a,b) and updated (c,d) versions of PWBM. Simulated mean ALT is taken as the 30 year average for the grid cell encompassing each respective CALM location. Mean biases (simulated minus observed ALT) from the prior version are  $-36$  cm and  $-27$  cm for the NNR and ERA-40 simulations, respectively. With the updated version, biases are  $-4.0$  cm and  $5.9$  cm for NNR and ERA-40, respectively. A systematic underestimation of ALT is evident in simulations with the prior version. It should be noted that a scale mismatch exists in any comparison involving grid-to-point observations. While the updated model simulates well the mean among the observed ALTs, it struggles with predictability. This shortcoming is not uncommon among numerical models which simulate active layer dynamics [Su *et al.*, 2005; Lawrence *et al.*, 2012]. In a study of ALT estimates across northern Alaska produced by three different models, Shiklomanov *et al.* [2007], found that large differences in ALT were attributable to the different approaches used for characterization of surface and subsurface conditions. Measured ALT can vary substantially over small distances. At any given location, ALT is influenced by several factors including thermal properties of soil, snow characteristics, vegetation type, and soil moisture amount. It has been shown that variations in ALT of up to 50% can occur over short distances [Nelson *et al.*, 1997].

[27] At the pan-Arctic scale, the PWBM captures well the north-south ALT gradient (Figure 9). Estimates range between 30 and 40 cm along the Arctic coast and

approach 1.5 m in parts of southern and western Siberia and central Canada. The simulation with NNR forcings (Figure 9a) produces slightly greater ALTs compared to the ERA-40 simulation (Figure 9b). Simulated permafrost areal extent is  $14.6$  ( $14.4$ – $14.8$ )  $\times 10^6$  km<sup>2</sup> and  $13.3$  ( $13.0$ – $13.6$ )  $\times 10^6$  km<sup>2</sup> from the NNR and ERA-40 simulations, respectively. This compares with an observed area of continuous plus discontinuous permafrost of  $12.5$  ( $11.8$ – $14.6$ )  $\times 10^6$  km<sup>2</sup> [Zhang *et al.*, 2000]. Thus, our simulated areas are 7 and 17% above observed extent for the ERA-40 and NNR simulations, respectively. However, as Lawrence *et al.* [2012] noted, permafrost area obtained from a coarse model is likely biased high. If true, the  $14.6 \times 10^6$  km<sup>2</sup> (continuous plus discontinuous permafrost) extent estimated by Zhang *et al.* [2000] would represent a better goal for model simulations.

[28] Figure 10 shows the results of a comparison between simulated runoff in the present study (labeled PWBM<sub>2013</sub>) and those described in Rawlins *et al.* [2003] (PWBM<sub>2003</sub>). Marked differences are evident. For the Yenisei, Lena, and Yukon basins, annual runoff in the present simulation is closer to observed values from the R-ArcticNet v4.0 archive (<http://www.r-arcticnet.sr.unh.edu/v4.0/>) [Lammers *et al.*, 2001]. For the Ob and Nelson basins, observed runoff is relatively low and simulated runoff is clearly overestimated. Annual observed runoff averaged over the pan-Arctic basin (1979–2001) is approximately  $230$  mm yr<sup>-1</sup> [Rawlins *et al.*, 2010]. Comparing this recent estimate to the 180

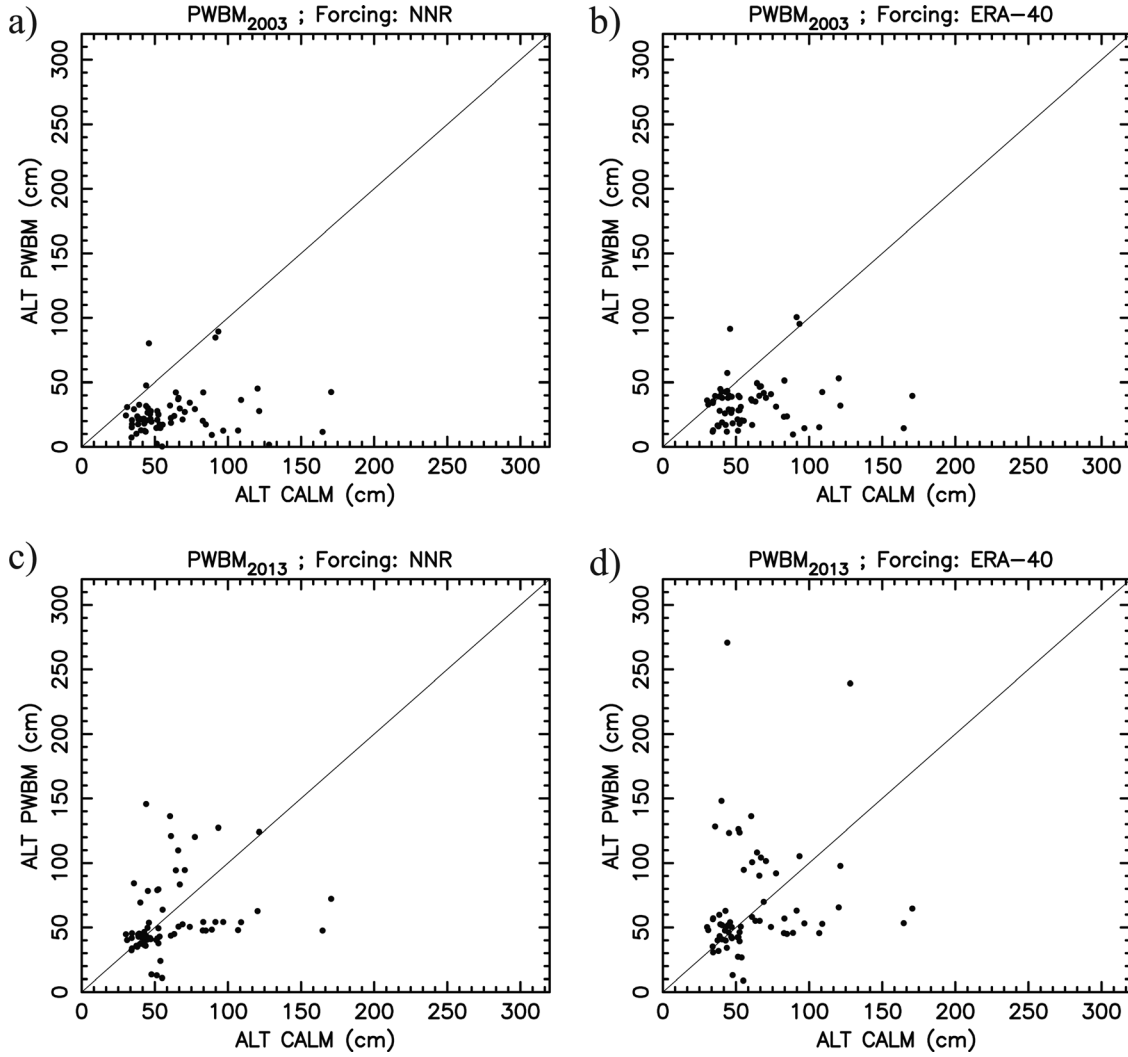


**Figure 8.** Scatter plot of CALM ALT and simulated ALT from the prior (PWBM<sub>2003</sub>)(a,b) and updated version of the PWBM (PWBM<sub>2013</sub>)(c,d). Observed ALT is the average for available years for each site. Mean bias is  $-4.0$  and  $5.9$  cm for the NNR and ERA-40 PWBM<sub>2013</sub> simulations, respectively. Mean bias is  $-36.5$  and  $-27.0$  for the NNR and ERA-40 PWBM<sub>2003</sub> simulations, respectively. CALM sites across the Tibetan Plateau were excluded from the evaluation.

mm yr<sup>-1</sup> (1980–2001) from *Rawlins et al.* [2003] gives a bias (predicted minus observed) of approximately  $-22\%$ . Using the same NNR data as *Rawlins et al.* [2003] in the updated PWBM gives an annual runoff of 250 mm yr<sup>-1</sup>, a bias of 9%. We note that the observed runoff/precipitation (R/P) ratio for the Nelson basins is low relative to other high latitude river basins.

[29] Figure 11 illustrates the differences in soil moisture distribution with depth between simulations with the updated and prior model versions. It shows soil moisture variations for the grid cell encompassing the Bonanza Creek site from simulations forced with the measured (site) daily air temperatures along with NNR precipitation and wind data. The soil profile in the new version exhibits expected patterns, with nearly saturated mineral soils above the permafrost (Figure 11a). Upper organic rich layers become wet following snowmelt and are considerably drier than the underlying mineral soils

in summer. ALT averages 68 cm, close to the mean observed value of 55 cm from the CALM data set. In the prior version of the model (Figure 11b), the ALT reaches approximately 30 cm each year. Soil moisture is lower as well. In the prior version, soil ice thaw was calculated based on the fraction of the layer which thaws on a given day. This results in relatively higher soil ice and, hence, lower soil water amounts through summer.

### 4.3. Potential Future Changes in Near Surface Conditions

[30] Lastly, we explored potential future changes in soil thermal and moisture regimes using data from the North American Regional Climate Change Assessment Program (NARCCAP, <https://www.narccap.ucar.edu/>). The NARCCAP [Mearns et al., 2007] is archiving outputs from a set of regional climate model (RCM) simulations over a domain spanning North America. The

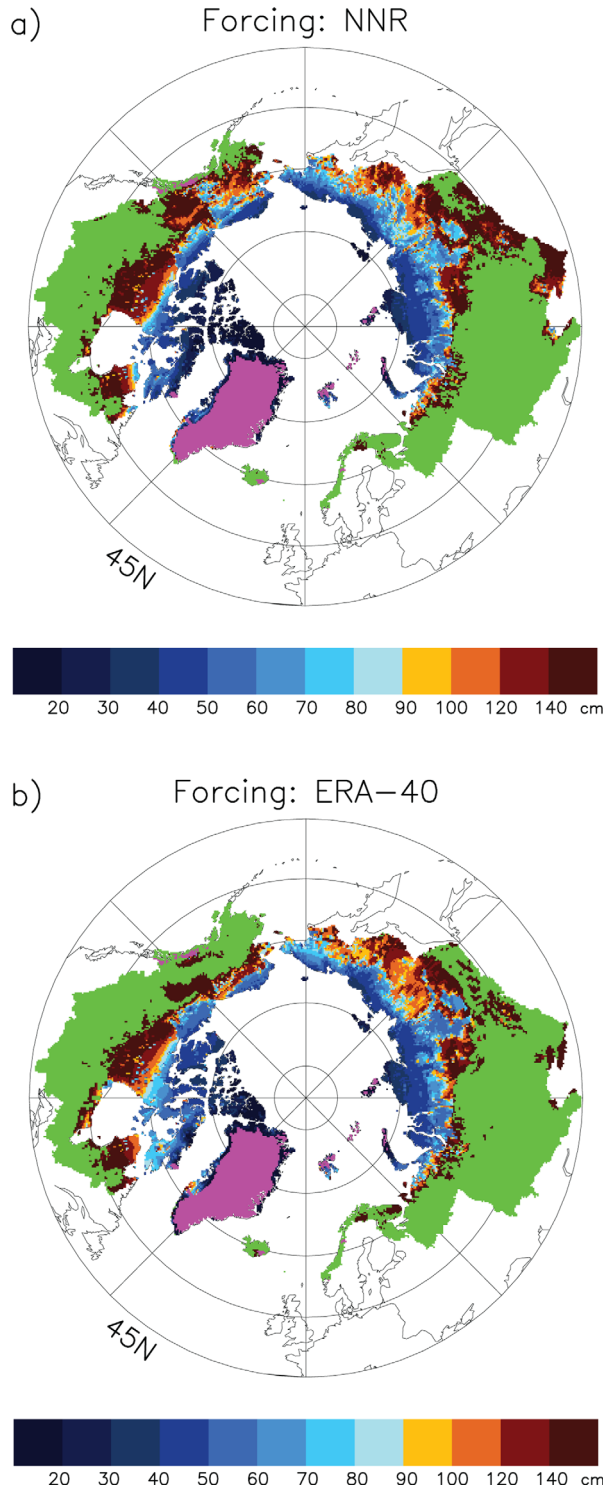


**Figure 9.** Simulated maximum seasonal active-layer thickness (ALT) for the period 1980–1999 for NNR (a) and ERA-40 (b). Areas shaded green and purple are nonpermafrost and glacier grid cells, respectively.

NARCCAP includes six RCMs, each forced with boundary conditions from two atmosphere-ocean general circulation models (GCMs). For each model pairing, air temperature and precipitation are available for

two 30 year periods: 1971–2000 and 2041–2070 (hereafter present and future, respectively). From the native RCM grids, we selected the cell which encompasses the Bonanza Creek area and averaged daily air temperature and precipitation across the available GCM-RCM pairings. Wind speed was taken as the daily climatology from the NRR data. Model spin-up for each 30 year simulation was performed by iterating over the first year of the present and future periods (1971 and 2041, respectively). For the grid chosen, a moderate cold and wet bias is present. To ameliorate the influence this bias would place on results we scaled each daily time series using monthly observations for Fairbanks International airport. Table 3 lists original and bias-adjusted values. Temperature change between the future and present periods is  $2.9^{\circ}\text{C}$  and precipitation change is just over 30%. As described below, our analysis of potential changes in ALT, thawed season length, soil temperature and moisture focuses on averages over the periods 1996–1999 and 2066–2069.

[31] Figure 12a shows simulated soil temperature as a function of depth for the period 1996–1999. Forcing the model with the bias-adjusted NARCCAP data results in a seasonally frozen (nonpermafrost) soil column. We note that average grid cell temperature over the 1971–1999 period with this simulation is just over  $1.5^{\circ}\text{C}$  warmer than the NNR and ERA-40 data. The absence of permafrost here is not entirely unexpected as the area around Bonanza Creek is in the discontinuous permafrost zone. For the present day simulation, the 30 cm soil layer is above  $0^{\circ}\text{C}$  for an average of 156 days (DOY 118–273). In the future simulation (Figure 12b), the thawed period increases to 166 days (DOY 115–280) and June–August temperature are warmer by  $1.9^{\circ}\text{C}$ . In the present simulation, soil temperatures at 45 cm are below  $0^{\circ}\text{C}$  for 158 days (late December to early June). In the future simulation frost does not reach 45 cm during winter. By the late 2060s, increased precipitation contributes to a deeper simulated snowpack, with depths in February and March greater by 26 and 28%, respectively (Figure 13b). The end of snowmelt advances by approximately 10 days (May 3 to April 23). For the present simulation soils between 30 and 40 cm thaw near DOY 160, experience recharge from above, and average 44% water content during the unfrozen period. In the future simulation, soil moisture averages 39%, with the 30 and 40 cm layer unfrozen all year. Soil moisture between 50 and 100 cm lowers from 58% to 54% in the future simulation.

## 5. Discussion

[32] The model simulations exhibit the temporal evolution of increasing snow density through winter, ranging between 100 and  $300\text{ kg m}^{-3}$  at the four Alaska study sites. The magnitude of simulated snow density and its time evolution are consistent with the expected performance based on prior research [Liston *et al.*, 2007; Schaefer *et al.*, 2009]. Our comparisons between simulated and observed soil temperatures at the four research sites documents that in most months the model

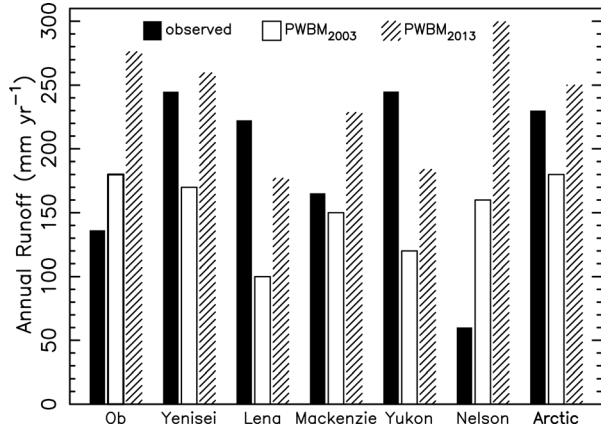


**Figure 10.** Annual average runoff for major river basins and the pan-Arctic (1980–1999) from gauged-based observations, the prior version (PWBm<sub>2003</sub>), and the new version (PWBm<sub>2013</sub>) of the PWBm. Observed discharge values were converted to unit depth runoff (mm yr<sup>-1</sup>) using discharge volume and basin area. Individual river basin discharge data come from the R-ArcticNet database. The pan-Arctic estimate is from Rawlins et al. [2010].

estimated temperatures generally fall in the range of observations. Over the four sites, PWBm simulated temperature at 25 and 50 cm falls within the observed range in 135 of the 244 site-months with sufficient observations (Figure 7). Temperatures in summer are well captured and rarely fall outside of the observed range. Biases occur mainly in winter, positive in some instances and negative in others. No systematic bias is noted. Our sensitivity experiments illustrate how errors in snow depth and organic layer thickness can explain much of the discrepancy between simulated and measured soil temperature. These results are consistent with recent research which has demonstrated the importance of realistic treatments of snowfall/density and organic layer thickness for simulations of the soil temperature regime. Previous research using the CLM has illustrated that precipitation biases can adversely affect simulations of the soil thermal regime and, in turn, permafrost extent [Lawrence et al., 2012]. Excessive snowfall and the resulting deeper snowpacks would lead to soils that are consistently too warm in winter. Our sensitivity tests for the Bonanza Creek sites indicate that differences in summer temperatures for the south-facing slope and spruce stands can be large due to differences in organic layer thickness and vegetation type.

[33] The pan-Arctic simulations provide additional information on model performance. When forced with ERA-40-derived air temperature and precipitation, the PWBm captures well the mean of the observed active layer thicknesses (ALT). Mean bias is 5.9 cm for the ERA-40 simulation and -4.0 cm for NNR. Predictability in ALT is limited. That said, ALT magnitudes in this new updated version of the model are close to measured values, whereas the earlier version of PWBm which used the Stefan solution shows a substantial low

bias. Grid-to-point comparisons are known to create interpretation problems. Moreover, the high degree of spatial variation in ALT over small distances [Nelson et al., 1998] due to several factors operating over small space scales [Shiklomanov and Nelson, 2002; Streletskiy et al., 2012] present obvious challenge for validations of large-scale LSMs and hydrology models. Nonetheless, the PWBm well estimates the spatial pattern and gradient in ALT across the pan-Arctic basin. In light of these results, we conclude that good agreement exists in permafrost extent from the two pan-Arctic simulations.

[34] When compared with the prior version of the model, simulated runoff is consistently higher across the major Arctic river basins. Better agreement with observed runoff is found for three (Lena, Yenisei and Yukon) of the six basins. Although considerable discrepancies are evident for the Ob and Nelson basins, pan-Arctic average runoff is improved. A large expanse of lakes, ponds, and wetlands that store and then evaporate runoff over the warm season characterize parts of the Ob basin. Land-surface models must capture this seasonal inundation and resultant enhanced evaporation in order to accurately simulate the regional water cycle. We speculate that incorporation of satellite-based products of inundated area [Schroeder et al., 2010] into

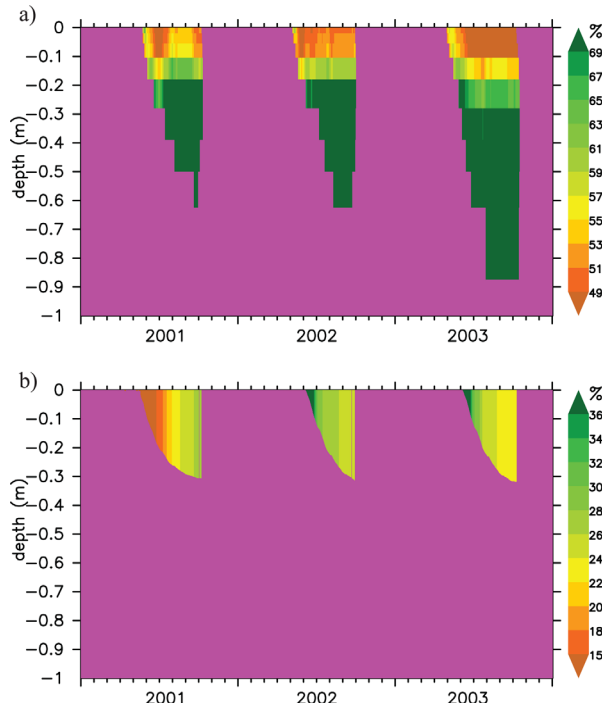


**Figure 11.** Simulated average daily soil moisture (% saturation  $S_w = \frac{\Theta}{\phi}$ , where  $\Theta$  is volumetric water content and  $\phi$  is porosity) for the Bonanza Creek grid cell for 2001–2003 from (a) the new updated version and (b) the prior version of the PWBm. Frozen ground is shaded purple. Air temperature forcing is taken as the average of the measured values across the Bonanza Creek sites (Table 2). Active layer thickness in the prior version of the PWBm is derived through application of the Stefan solution.

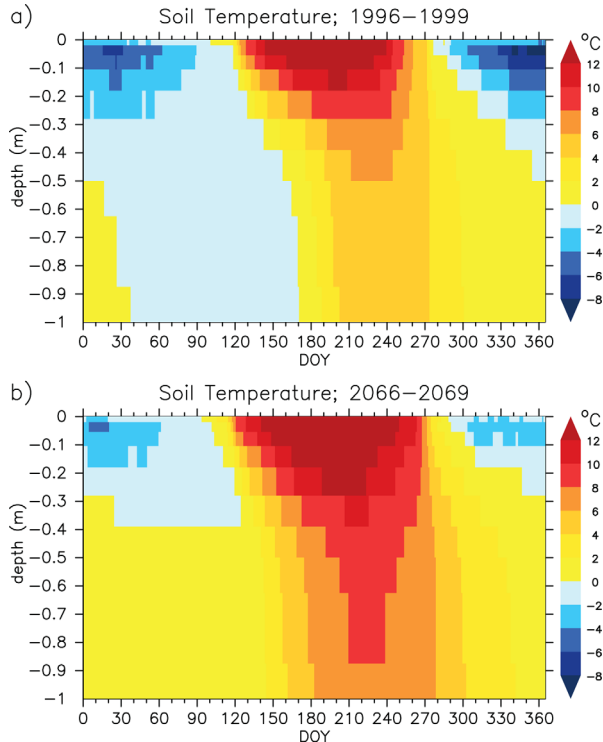
**Table 3.** Average Air Temperatures and Precipitation for the Grid Encompassing Bonanza Creek

Quantity	Average Temperature (°C)
NARCCAP average temperature (1971–2000)	−7.0
Observed temperature (1971–2000)	−1.4
Bias-adjusted temperature (1971–2000)	−1.3
Bias-adjusted temperature (2041–2070)	1.6

Quantity	Average Precipitation (mm yr <sup>−1</sup> )
NARCCAP average precipitation (1971–2000)	640
Observed precipitation (1971–2000)	320
Bias-adjusted precipitation (1971–2000)	360
Bias-adjusted precipitation (2041–2070)	470

models such as the PWBm and CLM may improve the timing of seasonal river discharge across this region. In the updated model, the new multiple layer configuration which incorporates the properties of organic soils is better able to resolve vertical soil moisture variations commonly found in permafrost regions. Additional evaluations of the seasonal cycle in simulated soil moisture, runoff, and river discharge will be the focus of future study.



**Figure 12.** Simulated daily soil temperature as a function of depth for the Bonanza Creek grid cell averaged over (a) 1996–1999 and (b) 2066–2069. Bias-adjusted forcings from the NARCCAP data set were applied in the simulation. Table 3 lists the air temperature and precipitation values. A 7 day running mean is applied to the simulated soil temperatures.

[35] Our final two simulations allowed us to explore potential connections between elements of the Arctic water cycle as the climate warms. For the period 2041–2070, the bias-adjusted NARCCAP data show warmer (by  $\sim 3^{\circ}\text{C}$ ) air temperatures and increased (by  $\sim 30\%$ ) precipitation for the region near Bonanza Creek in central Alaska. For the upper 30 cm of soil, the frost-free period increases by approximately 10 days. Higher precipitation rates lead to a deeper snowpack in early spring. However, as might be expected with warming, final snowmelt advances relative to the present period. Soil moisture at depth is lower in the future simulation. We find no significant change to evapotranspiration (ET) in the model simulation. Soil recharge following snowmelt is lower relative to the present day simulation. In effect, the increased winter precipitation stored at the surface as snow produces greater runoff at the expense of recharge with no net wetting of soils in early summer.

## 6. Summary

[36] In this study, we described new components of the PWBm and evaluated its performance against

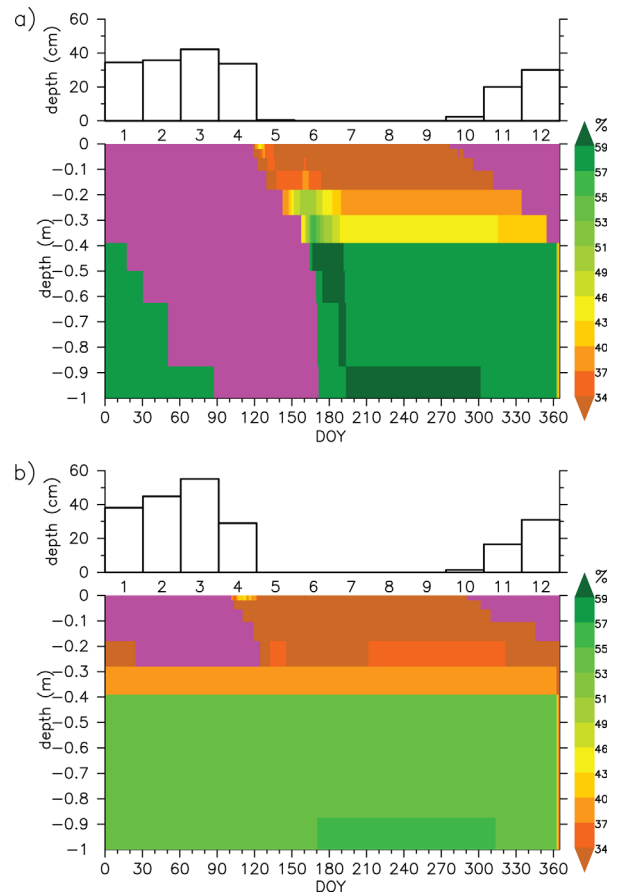


**Figure 13.** Simulated average daily soil moisture (%) saturation) and monthly average snow depth (bars, cm) for the Bonanza Creek grid cell over (a) 1996–1999 and (b) 2066–2069. A 7 day running mean is applied to the simulated soil temperatures. Purple shading indicates where soil temperatures are below  $0^{\circ}\text{C}$ .



observed data. Model improvements include a new multilayer soil model with increased total soil depth and representation of unfrozen water dynamics and phase change. The new soil model includes specifications of thermal and hydraulic properties of organic material in the column. Our new snow model simulates the effects of seasonal changes in snow density and, in turn, snow thermal conductivity.

[37] The results presented here illustrate how the PWBm is generally able to capture the range in soil temperatures observed over short distances. For the analysis of soil temperatures at the four study sites in Alaska, we observe no systematic bias. The sensitivity experiments suggest that much of the bias in simulated soil temperatures at depth can be explained by uncertainties in snowfall/snowdepth or organic layer thickness as reflected in model-layer carbon density. Comparisons of simulated ALT against measured values from the CALM network show limited agreement, a finding that has been observed in other recent studies. The simulated areal permafrost extent compares well with observed estimates. Although we observe large biases in simulated annual runoff for two of the six basins examined, our new estimates are nevertheless more consistent with pan-Arctic total runoff than the runoff amounts from the prior model version. Our simulations of potential future changes to the upper soil thermal and moisture regime highlight the importance of seasonality in a changing Arctic climate. While the considerable increase in annual precipitation is manifested in part as a deeper simulated snowpack in spring, soil moisture in summer tends to be lower. This suggests that much of the storage of water in snowpacks that may occur under an intensified hydrologic cycle could be partitioned to overland runoff at the expense of soil moisture recharge.

## Appendix A: Modeling of Soil Temperature

### A1. Model of Soil Freezing and Thawing

[38] In many practical applications, heat conduction is the dominant mode of energy transfer in ground materials. Within certain assumptions [Andersland and Anderson, 1978], the soil temperature  $T$ , [°C] can be simulated by a 1-D heat equation with phase change [Carslaw, 1974]:

$$C \frac{\partial}{\partial t} T(z, t) + L \zeta \frac{\partial}{\partial t} \theta(T, z) = \frac{\partial}{\partial z} \left( \lambda \frac{\partial}{\partial z} T(z, t) \right), \quad (A1)$$

$$z \in [z_s, z_b], t \in [0, \tau].$$

[39] The quantities  $C = C(T, z)$  [ $Jm^{-3}K^{-1}$ ] and  $\lambda = \lambda(T, z)$  [ $Wm^{-1}K^{-1}$ ] represent the volumetric heat capacity and thermal conductivity of soil, respectively;  $L$  [ $Jm^{-3}$ ] is the volumetric latent heat of fusion of water,  $\zeta$  is the volumetric water content, and  $\theta$  is the unfrozen liquid pore water fraction. The volumetric water content  $\zeta = \eta \chi$ , where  $\eta$  is the soil porosity and  $\chi \in [0, 1]$  is the fraction of voids filled with water. The latter can be obtained by solving the Richard's equation (see equation (2) in section 2.1.).

[40] The heat equation is supplemented by initial temperature distribution  $T(z_s, 0) = T_0(z)$ , and boundary conditions at the snow/ground surface  $z_s$  and at the depth  $z_b$ . Here,  $T_0(z)$  is the temperature at  $z \in [z_s, z_b]$  at time  $t = 0$ ;  $T_{air}$  is observed air temperatures at the ground/snow surface, respectively. We use the Dirichlet boundary conditions at the snow surface, i.e.,  $T(z_s, t) = T_{air}(t)$ , and a heat flux boundary condition at the bottom of the soil column  $\lambda \nabla T(l, t) = \mathcal{G}$ , where  $\mathcal{G}$  is the geothermal heat flux. In the model we assume that the lower boundary  $z_b$  is located at 60.0 m, a depth that is adequate to simulate temperature dynamics on the decadal scale [Alexeev et al., 2007].

### A2. Snow Model

[41] The snow model in PWBm leverages approaches described in Schaefer et al. [2009] and Liston et al. [2007]. It incorporates the Sturm et al. [1995] snow classification. To resolve temperature dynamics, the snow model simulates up to five layers depending on total depth. The bottom layer is thickest with decreasing layer thickness moving upward. Within this framework, we impose a two-layer density model which is conceptually similar to the approach used in the SiBCASA as described in Schaefer et al. [2009]. The relative thickness of the bottom depth hoar layer ( $f_{bot}$ ) is a function of total snowpack depth

$$f_{bot} = f_{botmax} / (1 + \exp(D_{slope}(D_{half} - D))) \quad (A2)$$

where  $f_{botmax}$  is the maximum potential thickness for the depth hoar layer and  $D_{slope}$  and  $D_{half}$  are  $f_{bot}$  slope and half point

$$\begin{aligned} D_{half} &= (D_{max} + D_{min})/2 \\ D_{slope} &= 10 / (D_{max} + D_{min}) \end{aligned} \quad (A3)$$

[42] Here  $D_{min}$  is the minimum depth where a bottom layer forms and  $D_{max}$  is the depth where  $f_{bot}$  is its maximum value. Within the global snow classification of Sturm et al. [1995], only tundra and taiga types occur across the pan-Arctic drainage basin. For tundra grids,  $D_{min}$ ,  $D_{max}$ , and  $f_{botmax}$  are 0.0, 0.1, and 0.3, respectively [Schaefer et al., 2009]. For taiga snow, they are 0.0, 0.7, and 0.7. Due to the special properties of the depth hoar layer in tundra and taiga environments, we assume thermal conductivity ( $\lambda_{dh}$ ) in this layer as 0.18 and 0.072  $W m^{-2} K^{-1}$ , respectively. Temporal evolution of density in the upper “soft snow” layer are calculated based on the approach described in Liston et al. [2007], wherein snow density is influenced primarily through snow precipitation and compaction as a result of wind. New snow density is defined

$$\rho_{ns} = \rho_0 + 1.7(T_a - 258.16)^{1.5} \quad (A4)$$

where  $T_a$  is air temperature and  $\rho_0$  is fresh snow. Here we use a value of 100  $kg m^{-3}$  as opposed to the 50  $kg m^{-3}$  applied in Liston et al. [2007]. A density offset is added for wind speeds  $> 5 m s^{-1}$ . During periods of no precipitation snow density evolution is given by

$$\frac{d\rho_s}{dt} = CA_1 U \rho_s \exp[-B(T_f - T_s)] \exp(-A_2 \rho_s) \quad (\text{A5})$$

where  $T_f$  is freezing temperature,  $T_s$  is soft snow temperature,  $B$  is a constant equal to  $0.08 \text{ K}^{-1}$ ,  $A_1$  and  $A_2$  are constants set to  $0.0013 \text{ m}^{-1}$  and  $0.021 \text{ m}^3 \text{ kg}^{-1}$ , respectively, and  $C = 0.10$  is a constant that controls the snow density change rate. Thermal conductivity of the upper snow layer for both tundra and taiga classes is

$$\lambda_{\text{eff}} = 0.138 - 1.01 \rho_s + 3.233 \rho_s^2 \quad (\text{A6})$$

where  $\lambda_{\text{eff}}$  is in  $\text{W m}^{-1} \text{ K}^{-1}$  and  $\rho_s$  is snow density in  $\text{kg m}^{-3}$  [Sturm et al., 1997]. We assumed a thermal conductivity in the lower depth hoar layer of  $0.18 \text{ W m}^{-1} \text{ K}^{-1}$  for tundra snow and  $0.072 \text{ W m}^{-1} \text{ K}^{-1}$  for taiga snow. Finally, the snow thickness  $z_s = z_s(t)$  is computed simply using the model estimate for snow water equivalent  $W$  and snow density  $z_s(t) = W/\rho_s$ .

### A3. Parameterization of the Soil Properties

[43] We adopt the parameterization of thermal properties proposed by DeVries [1963] and Sass et al. [1971] with some modifications and thus define the thermal conductivity  $\lambda_m$  as well as the heat capacity  $C_m$  for the mineral soil by

$$\lambda = \lambda_s^{1-\eta} [\lambda_a^{1-\chi} \lambda_w^\chi]^\eta, \quad \lambda_w = \lambda_l^\theta \lambda_i^{1-\theta}, \quad (\text{A7})$$

and

$$C = (1-\eta)C_s + \eta[(1-\chi)C_a + \chi C_w], \quad C_w = \theta C_l + (1-\theta)C_i, \quad (\text{A8})$$

where  $C_k$  and  $\lambda_k$ ,  $k \in \{a, w, i, s\}$  are the volumetric heat capacities and the thermal conductivities of the  $k$ th component, respectively. Subscripts “s”, “a”, “w”, “l”, and “i” stand for the skeleton (mineral and organic), air, water, liquid water and ice, respectively.

[44] Following Lawrence and Slater [2008], the volumetric heat capacity  $C_s$  is a weighted combination of the capacities for the organic and mineral parts, i.e.,  $C_s = (1-f)C_m + fC_o$ , where  $f$  is the fraction of organic material in the soil, and  $C_m$  and  $C_o$  are the volumetric heat capacities of the mineral and organic soil skeleton, respectively. However, we use geometric averaging to compute  $\lambda_s$  as follows:  $\lambda_s = \lambda_m^{1-f} \lambda_o^f$ , where  $\lambda_o$  is the thermal conductivity of the organic layer, and  $\lambda_s$  is the thermal conductivity of the mineral soil skeleton. Values of  $C_m$  and  $\lambda_m$  are listed in Table 1. We assume here that the thermal conductivity  $\lambda_o$  and volumetric heat capacity  $C_o$  of the organic layer with zero porosity is  $1.5 \text{ W m}^{-1} \text{ K}^{-1}$  and  $1.9 \times 10^6 \text{ J m}^{-3} \text{ K}^{-1}$ , respectively.

[45] Recall that the value of  $\theta \in [0, 1]$  stands for the unfrozen liquid pore water fraction. There are many approximations to  $\theta$  for fully saturated soil ( $\chi = 1$ ). The most common approximations are associated with power or exponential functions. Based on prior work, we parameterize  $\theta$  by a power function  $\theta(T) = a|T|^{-b}$ ;

$a, b > 0$  for  $T < T_* < 0^\circ \text{C}$ . The constant  $T_*$  is the freezing point depression. However, in thawed soils ( $T > T_*$ ), all pore water is liquid and thus  $\theta = 1$ . We thus hypothesize that the assumptions

$$\theta = \begin{cases} 1, & T \geq T_* \\ |T_*|^b |T|^{-b}, & T < T_* \end{cases}, \quad (\text{A9})$$

are valid both for the saturated and partially saturated soils. Small values of  $b$  describe the liquid water content in fine-grained soils, whereas large values of  $b$  are related to coarse-grained materials in which almost all water freezes at the temperature  $T_*$ .

#### A3.1. Determination of Snow Layers

[46] For the sake of computational efficiency, we discretize the soil column  $[0, z_b]$  into 22 layers and the snow pack  $[z_s, 0]$  into up to five layers depending on the value of  $z_s$  as discussed below.

[47] A space above the ground surface is split into five fixed layers  $z_{-5} = -0.70 \text{ m}$ ,  $z_{-4} = -0.45 \text{ m}$ ,  $z_{-3} = -0.30 \text{ m}$ ,  $z_{-2} = -0.15 \text{ m}$ , and  $z_{-1} = -0.07 \text{ m}$ . For example, when the snow pack thickness  $z_s$  is  $0.3 \text{ m}$ , then the snow consists of three layers  $z_{-3}$ ,  $z_{-2}$ ,  $z_{-1}$ . Under added snow thickness  $z_s$  increases and it exceeds  $z_{-3}$ . To take into account this fresh snow, the value of  $z_{-3}$  is dynamically adjusted to become the current snow thickness. Note that the number of snow layers is still equal to three. However, when the snowpack thickness becomes larger than  $(z_{-3} + z_{-4}/2)$ , a fourth layer is added where  $z_{-1} = -0.07$ ,  $z_{-2} = -0.15$ ,  $z_{-3} = -0.30$ , and  $z_{-4} = z_s$ . The thermal conductivity and heat capacity for each layer is the same and defined by equation (2).

#### A3.2. Numerical Implementation

[48] Following a finite element framework [Zienkiewicz and Taylor, 1991], we approximate  $T(z, \tau) \approx \sum_{i=1}^n \phi_i(z) \mathbf{t}_i(\tau)$ , where  $\mathbf{t}_i(\tau)$  is a “value” of temperature at the  $i$ th finite element grid, and  $\phi_i$  is the so-called basis function. After some standard manipulations, we derive a system of differential equations.

$$\mathbf{M}(\mathbf{t}) \frac{d}{d\tau} \mathbf{t}(\tau) = -\mathbf{K}(\mathbf{t}) \mathbf{t}(\tau), \quad \mathbf{t} = \mathbf{t}(\tau), \quad (\text{A10})$$

where  $\mathbf{t}(\tau) = \{\mathbf{t}_i(\tau)\}_{i=1}^n$  is the vector consisting of temperature values,  $\mathbf{M}(\mathbf{t}) = \{m_{ij}(\mathbf{t})\}_{ij=1}^n$  and  $\mathbf{K}(\mathbf{t}) = \{k_{ij}(\mathbf{t})\}_{ij=1}^n$  are the  $n \times n$  capacitance and stiffness matrices, respectively. A further refinement, which is often used in finite element modeling of phase change problems, is to exploit a so-called “lumped” formulation, i.e., the capacitance matrix  $\mathbf{M}$  is diagonal:

$$m_{ij}(\mathbf{t}) = \delta_{ij} c_i(\mathbf{t}) \int_0^l \psi_i dx, \quad c_i(\mathbf{t}) \approx C(\mathbf{t}_i, z_i) + L \zeta_i \frac{d\theta}{dT}(\mathbf{t}_i), \quad (\text{A11})$$

where  $\delta_{ij}$  is one if  $i = j$ , or zero otherwise. Dalhuijsen and Segal [1986] provides justification for the lumped formulation, noting that it is computationally advantageous and avoids oscillations in numerical solutions when used in conjunction with the backward Euler scheme:

$$\begin{aligned} \left[ \mathbf{M}^{(k)} + d\tau_k \mathbf{K}^{(k)} \right] \mathbf{t}^{(k)} &= \mathbf{M}^{(k)} \mathbf{t}^{(k-1)}, & k > 1 \\ \mathbf{t}^{(k)} &= \mathbf{t}_0, & k = 0. \end{aligned} \quad (\text{A12})$$

[49] The main difficulty in numerical modeling of soil freezing/thawing involves the consistent calculation of the derivative  $d\theta/dT$  in equation (A11), where  $\theta(T)$  is not a continuously differentiable function defined by equation (A9). In many reviews, it is proposed to employ the enthalpy temporal averaging to calculate  $c_i(\mathbf{t})$ . We suggest an approach that incorporates ideas of temporal averaging just to evaluate the rapidly changing  $\theta(T)$  by defining  $c_i$  as

$$c_i(\mathbf{t}^{(k)}) = C(\mathbf{t}_i^{(k)}, z_i) + L \frac{\theta_r(\mathbf{t}_i^{(k)}) - \theta_r(\mathbf{t}_i^{(k-1)})}{\mathbf{t}_i^{(k)} - \mathbf{t}_i^{(k-1)}}. \quad (\text{A13})$$

[50] We note that an advantage of this definition is that it does not compute temporal averaging of the heat capacity, and hence reduces numerical computations, and at the same time preserves numerical accuracy of the original idea. The interested reader is directed to *Nicolsky et al.* [2007, 2009] for further details about the phase change computations.

[51] **Acknowledgments.** This research was supported by the U.S. National Aeronautics and Space Administration NASA grant (NNX11AR16G). The authors thank two anonymous reviewers and the Associate Editor for their constructive comments. We thank the North American Regional Climate Change Assessment Program (NARCCAP) for providing data used in this paper. NARCCAP is funded by the National Science Foundation (NSF), the U.S. Department of Energy (DoE), the National Oceanic and Atmospheric Administration (NOAA), and the U.S. Environmental Protection Agency Office of Research and Development (EPA). Portions of this work were performed at the Jet Propulsion Laboratory, California Institute of Technology, under contract with the National Aeronautics and Space Administration.

## References

- Alexeev, V. A., D. J. Nicolsky, V. E. Romanovsky, and D. M. Lawrence (2007), An evaluation of deep soil configurations in the CLM3 for improved representation of permafrost, *Geophys. Res. Lett.*, **34**, L09502, doi:10.1029/2007GL029536.
- Andersland, O., and D. Anderson (1978), *Geotechnical Engineering for Cold Regions*, McGraw-Hill, New York.
- Brown, J., K. M. Hinkel, and F. E. Nelson (2000), The circumpolar active layer monitoring (CALM) program, *Polar Geogr.*, **24**(3), 165–258.
- Callaghan, T. V., M. Johansson, O. Anisimov, H. H. Christiansen, A. Instanes, V. Romanovsky, and S. Smith (2011), Chapter 5: Changing permafrost and its impacts. In *Snow, Water, Ice and Permafrost in the Arctic (SWIPA)*, Arctic Monitoring and Assessment Programme (AMAP), Oslo.
- Carlsaw, H. S., and J. C. Jaeger (1959), *Conduction of Heat in Solids*, Oxford Univ. Press, New York, pp. 302, 340–341.
- Christiansen, H. H., et al. (2010), The thermal state of permafrost in the Nordic area during the international polar year 2007–2009, *Permafrost Periglac. Processes*, **21**(2), 156–181, doi:10.1002/ppp.687.
- Clilverd, H. M., D. M. White, A. C. Tidwell, and M. A. Rawlins (2011), The sensitivity of northern groundwater recharge to climate change: A case study in Northwest Alaska, *J. Am. Water Resour. Assoc.*, **47**, 1–13.
- Dalhuisen, A., and A. Segal (1986), Comparison of finite element techniques for solidification problems, *Int. J. Numer. Methods. Eng.*, **23**(10), 1807–1829.

- DeVries, D. (1963), Thermal properties of soils, in *Physics of Plant Environment*, edited by W. R. van Wijk, pp. 210–235, North-Holland, Amsterdam.
- Farouki, O. T. (1981), The thermal properties of soils in cold regions. *Cold Regions Science and Technology*, **5**(1), 67–75.
- Frey, K. E., and J. W. McClelland (2009), Impacts of permafrost degradation on arctic river biogeochemistry, *Hydrol. Processes*, **23**, 169–182, doi:10.1002/hyp.7196.
- Global Soil Data Task (2000), Global gridded surfaces of selected soil characteristics (IGBP-DIS). International Geosphere-Biosphere Programme Data and Information Services, Oak Ridge National Laboratory, Oak Ridge, Tennessee, USA, available online at: <http://www.daac.ornl.gov/> (last access: February 2003) from the ORNL Distributed Active Archive Center.
- Hinzman, L. D. (2005), Evidence and implications of recent climate change in Northern Alaska and other Arctic regions, *Clim. Change*, **72**(3), 251–298, doi:10.1007/s10584-005-5352-2.
- Jiang, Y., Q. Zhuang, and J. A. O'Donnell (2012), Modeling thermal dynamics of active layer soils and near-surface permafrost using a fully coupled water and heat transport model, *J. Geophys. Res.*, **117**, D11110, doi:10.1029/2012JD017512.
- Kalnay, E., et al. (1996), The NCEP/NCAR 40-year reanalysis project, *Bull. Am. Meteorol. Soc.*, **77**(3), 437–471.
- Lammers, R. B., A. I. Shiklomanov, C. J. Vörösmarty, B. M. Fekete, and B. J. Peterson (2001), Assessment of contemporary Arctic river runoff based on observational discharge records, *J. Geophys. Res.*, **106**(D4), 3321–3334.
- Lawrence, D. M., and A. G. Slater (2008), Incorporating organic soil into a global climate model, *Clim. Dyn.*, **30**, doi:10.1007/s00382-007-0278-1.
- Lawrence, D. M., A. G. Slater, and S. Swenson (2012), Simulation of present-day and future permafrost and seasonally frozen ground conditions in CCSM4, *J. Clim.*, **25**, 2207–2225, doi:10.1175/JCLI-D-11-00334.1.
- Liston, G. E., R. B. Haehnel, M. Sturm, C. A. Hiemstra, S. Berezovskaya, and R. D. Tabler (2007), Simulating complex snow distributions in windy environments using SnowTran-3D, *J. Glaciol.*, **53**(181), 241–256.
- Matsuura, K., and C. J. Willmott (2009), *Terrestrial Air Temperature: 1900–2008 Gridded Monthly Time Series*, Version 2.01. [Available at <http://climate.geog.udel.edu/~climate/>].
- Mearns, L. O., et al. (2007), updated 2012. The North American Regional Climate Change Assessment Program dataset, National Center for Atmospheric Research Earth System Grid data portal, Boulder, CO. Data downloaded 2013-08-20. [doi:10.5065/D6RN35ST].
- Nelson, F. E., N. I. Shiklomanov, G. R. Mueller, K. M. Hinkel, D. A. Walker, and J. G. Bockheim (1997), Estimating active-layer thickness over a large region: Kuparuk River Basin, Alaska, U.S.A., *Arc. Alp. Res.*, **29**, 367–378.
- Nelson, F. E., N. I. Shiklomanov, G. R. Mueller, L. L. Miller, and D. A. Walker (1998), Active-layer thickness in north-central Alaska: Systematic sampling, scale, and spatial autocorrelation, *J. Geophys. Res.*, **103**(D22), 28,963–28,973.
- Nicolsky, D., V. Romanovsky, V. Alexeev, and D. Lawrence (2007), Improved modeling of permafrost dynamics in a GCM land-surface scheme, *Geophys. Res. Lett.*, **34**, L08501, doi:10.1029/2007GL029525.
- Nicolsky, D., V. Romanovsky, and G. Panteleev (2009), Estimation of soil thermal properties using in-situ temperature measurements in the active layer and permafrost, *Cold Reg. Sci. Technol.*, **55**(1), 120–129, doi:10.1016/j.coldregions.2008.03.003.
- Oleson, K. W., G. B. Bonan, Coauthors et al. (2010), Technical description of version 4.0 of the community land model (CLM). NCAR Tech. Note NCAR/TN-4781STR. Boulder, Colorado.
- Peterson, B. J., R. M. Holmes, J. W. McClelland, C. J. Vörösmarty, R. B. Lammers, A. I. Shiklomanov, I. A. Shiklomanov, and S. Rahmstorf (2002), Increasing river discharge to the Arctic Ocean, *Science*, **298**, 2171–2173.
- Peterson, B. J., J. McClelland, R. Curry, R. M. Holmes, J. E. Walsh, and K. Aagaard (2006), Trajectory shifts in the Arctic and sub-Arctic freshwater cycle, *Science*, **313**, 1061–1066.
- Rawlins, M. A., R. B. Lammers, S. Frolking, B. M. Fekete, and C. J. Vörösmarty (2003), Simulating pan-Arctic runoff with a macro-

- scale terrestrial water balance model, *Hydrol. Processes*, 17, 2521–2539.
- Rawlins, M. A., M. Fahnestock, S. Frolking, and C. J. Vörösmarty (2007), On the evaluation of snow water equivalent estimates over the terrestrial Arctic drainage basin, *Hydrol. Processes*, 21(12), 1616–1623, doi:10.1002/hyp.6724.
- Rawlins, M. A., M. C. Serreze, R. Schroeder, X. Zhang, and K. C. McDonald (2009), Diagnosis of the record discharge of Arctic-draining Eurasian Rivers in 2007, *Environ. Res. Lett.*, 4, 045011, doi:10.1088/1748-9326/4/4/045011.
- Rawlins, M. A., et al. (2010), Analysis of the Arctic system for freshwater cycle intensification: Observations and expectations, *J. Clim.*, 23, 5715–5737.
- Rinke, A., P. Kuhry, and K. Dethloff (2008), Importance of a soil organic layer for Arctic climate: A sensitivity study with an Arctic RCM, *Geophys. Res. Lett.*, 35, L13709, doi:10.1029/2008GL034052.
- Romanovsky, V. E., S. L. Smith, and H. H. Christiansen (2010a), Permafrost thermal state in the polar Northern Hemisphere during the international polar year 2007–2009: A synthesis, *Permafrost Periglac. Processes*, 21(2), 106–116, doi:10.1002/ppp.689.
- Romanovsky, V. E., et al. (2010b), Thermal state of permafrost in Russia, *Permafrost Periglac. Processes*, 21(2), 136–155, doi:10.1002/ppp.683.
- Sass, J., A. H. Lachenbruch, and R. J. Munroe (1971), Thermal conductivity of rocks from measurements on fragments and its application to heat-flow determinations, *J. Geophys. Res.*, 76(14), 3391–3401.
- Schaefer, K., T. Zhang, A. G. Slater, L. Lu, A. Etringer, and I. Baker (2009), Improving simulated soil temperatures and soil freeze/thaw at high-latitude regions in the Simple Biosphere/Carnegie-Ames-Stanford Approach model, *J. Geophys. Res.*, 114, F02021, doi:10.1029/2008JF001125.
- Schaefer, K., T. Zhang, L. Bruhwiler, and A. Barrett (2011), Amount and timing of permafrost carbon release in response to climate warming, *Tellus, Ser. B*, 63, 165–180.
- Schroeder, R., K. C. McDonald, R. Zimmerman, E. Podest, and M. Rawlins (2010), North Eurasian inundation mapping with passive and active microwave remote sensing, *Environ. Res. Lett.*, 5, 015003, doi:10.1088/1748-9326.
- Serreze, M. C., et al. (2000), Observational evidence of recent change in the Northern high-latitude environment, *Clim. Change*, 46, 159–207.
- Shiklomanov, N. I., and F. E. Nelson (2002), Active-layer mapping at regional scales: A 13-year spatial time series for the Kuparuk region, north-central Alaska, *Permafrost Periglac. Processes*, 13(3), 219–230, doi:10.1002/ppp.425.
- Shiklomanov, N. I., O. A. Anisimov, T. Zhang, S. Marchenko, F. E. Nelson, and C. Oelke (2007), Comparison of model produced active layer fields: Results for northern Alaska, *J. Geophys. Res.*, 112, F02S10, doi:10.1029/2006JF000571.
- Smith, L. C., T. M. Pavelsky, G. M. MacDonald, A. I. Shiklomanov, and R. B. Lammers (2007), Rising minimum daily flows in northern Eurasian rivers: A growing influence of groundwater in the high-latitude hydrologic cycle, *J. Geophys. Res.*, 112, G04S47, doi:10.1029/2006JG000327.
- Smith, S., V. Romanovsky, A. Lewkowicz, C. Burn, M. Allard, G. Clow, K. Yoshikawa, and J. Throop (2010), Thermal state of permafrost in North America: A contribution to the international polar year, *Permafrost Periglac. Processes*, 21(2), 117–135, doi:10.1002/ppp.690.
- Streletskiy, D. A., N. I. Shiklomanov, and F. E. Nelson (2012), Spatial variability of permafrost active-layer thickness under contemporary and projected climate in Northern Alaska, *Polar Geogr.*, 35(2), 95–116.
- Sturm, M., J. Holmgren, M. König, and K. Morris (1997), The thermal conductivity of seasonal snow, *J. Glaciol.*, 43(143), 26–41.
- Sturm, M. J., J. Holmgren, and G. E. Liston (1995), A seasonal snow cover classification system for local to global applications, *J. Climate*, 8(5), 1261–1283.
- Su, F., J. C. Adam, L. C. Bowling, and D. P. Lettenmaier (2005), Streamflow simulations of the terrestrial Arctic domain, *J. Geophys. Res.*, 110, D08112, doi:10.1029/2004JD005518.
- Swenson, S. C., D. M. Lawrence, and H. Lee (2012), Improved simulation of the terrestrial hydrological cycle in permafrost regions by the community land model, *J. Adv. Model. Earth Syst.*, 4, M08002, doi:10.1029/2012MS000165.
- Uppala, S. M., et al. (2005), The ERA-40 re-analysis, *Q. J. R. Meteorol. Soc.*, 131(612), 2961–3012.
- Vörösmarty, C. J., B. Moore III, A. L. Grace, M. P. Gildea, J. M. Melillo, B. J. Peterson, E. B. Rastetter, and P. A. Steudler (1989), Continental scale models of water balance and fluvial transport: An application to South America, *Global Biogeochem. Cycles*, 3(3), 241–265.
- White, D., et al. (2007), The Arctic freshwater system: Changes and impacts, *J. Geophys. Res.*, 112, G04S54, doi:10.1029/2006JG000353.
- Willmott, C. J., and K. Matsuura (1995), Smart interpolation of annually averaged air temperature in the United States, *J. Appl. Meteorol.*, 34, 811–816.
- Willmott, C. J., and K. Matsuura (2000), Terrestrial Air Temperature and Precipitation: Monthly and Annual Time Series 1950–1999. WWW url: [http://climate.geog.udel.edu/~climate/html\\_pages/README.ghcn\\_ts.html](http://climate.geog.udel.edu/~climate/html_pages/README.ghcn_ts.html).
- Willmott, C. J., and S. M. Robeson (1995), Climatologically aided interpolation (CAI) of terrestrial air temperature, *Int. J. Climatol.*, 15, 221–229.
- Wisser, D., S. Marchenko, J. Talbot, C. Treat, and S. Frolking (2011), Soil temperature response to 21st century global warming: The role of and some implications for peat carbon in thawing permafrost soils in North America, *Earth Syst. Dyn.*, 2, 1–18.
- Wu Q., and Zhang T., (2010), Changes in active layer thickness over the Qinghai-Tibetan Plateau from 1995 to 2007, *J. Geophys. Res.*, 115, D09107, doi:10.1029/2009JD012974.
- Yoshikawa, K., and L. D. Hinzman (2003), Shrinking thermokarst ponds and groundwater dynamics in discontinuous permafrost near council, Alaska, *Permafrost Periglac. Processes*, 14(2), 151–160.
- Zhang, T. (2005), Influence of the seasonal snow cover on the ground thermal regime: An overview, *Rev. Geophys.*, 43, RG4002, doi:10.1029/2004RG000157.
- Zhang, T., J. A. Heginbottom, R. G. Barry, and J. Brown (2000), Further statistics on the distribution of permafrost and ground ice in the northern hemisphere, *Polar Geogr.*, 24, 126–131.
- Zhang, T., et al. (2005), Spatial and temporal variability in active layer thickness over the Russian Arctic drainage basin, *J. Geophys. Res.*, 110, D16101, doi:10.1029/2004JD005642.
- Zienkiewicz, O., and R. Taylor (1991), *The Finite Element Method. Solid and Fluid Mechanics, Dynamics and Nonlinearity*, vol. II, pp. 227–229, McGraw-Hill, New York.
- Zinke, P. J., A. G. Stangenberger, W. M. Post, W. R. Emanuel, and J. S. Olson (1986), Worldwide Organic Carbon and Nitrogen Data, Tech. Rep. ORNL/CDIC-18, Carbon Dioxide Inf. Cent., Oak Ridge, Tenn.

Corresponding author: M. A. Rawlins, Climate System Research Center, Department of Geosciences, University of Massachusetts, 611 North Pleasant St., Amherst, MA 01002, USA. (rawlins@geo.umass.edu)